Compact 1.31 μm-emission $In_{0.45}Ga_{0.55}As$/ $In_{0.25}Ga_{0.75}As$ photonic crystal nano-ridge laser monolithically grown on 300 mm silicon substrate

Z. Ouyang*[a], D. Colucci[b], E. M. B. Fahmy [a], A. A. Yimam [a], J. Van Campenhout[b], B. Kunert [b] and D. Van Thourhout[a]

[a]Dept. of INTEC, Gent University-imec, iGent, Technologiepark-Zwijnaarde 126, 9052 Gent, Belgium; [b]IMEC, kapeldreef 75, 3001 Heverlee, Belgium

ABSTRACT

Compact on-chip sources with efficient emission in the O-band are a critical component for the silicon photonics platform to realize its full potential in telecom and datacom applications. III-V semiconductors are still the main candidates for realizing such sources but their significant lattice mismatch with silicon remains a fundamental challenge hampering monolithic integration. Hence, we need innovative methods to confine defects outside the active device region. Here, an ultra-compact 1.31 μm-emission photonic crystal (PC) nano-ridge laser selectively area grown on a trench-patterned silicon substrate using aspect ratio trapping and nano-ridge engineering is demonstrated. Lasing at a remarkably low pumping threshold of 4.42 kW/cm^2 and with a cavity length as small as 50 μm was realized with the PC nano-ridge device. The laser exhibits a lasing peak with side-mode suppression ratio of over 17 dB and a linewidth as narrow as 1.47 nm under 22.91 kW/cm^2 pulsed pumping. This PC nano-ridge laser opens a novel route to realize a compact light source for future high-density and massively scalable silicon photonic integrated circuits in the field of data communication.

Keywords: compact, telecom and datacom, III-V semiconductors, aspect ratio trapping, nano-ridge engineering, high-density, massively-scalable.

1. INTRODUCTION

The global internet traffic keeps growing explosively, driven by a sustained growth in the performance of the underpinning technology. Cost-effective and low-power-dissipation chip-to-chip and on-chip optical interconnections are key to meet the demand for high-speed and high-performance optical communication [1]. The silicon photonics platform is emerging as a promising solution to address this challenge. Over the past decades, silicon photonics technology has shown steady progress, featuring keystone developments such as low-loss waveguides, ultra-fast modulators and high bandwidth detectors [2-4]. However, the absence of an efficient and compact optical emitter integrated on the silicon photonics platform remains a challenge. Various integration approaches for bringing III-V materials on silicon have been investigated, to overcome silicon's indirect bandgap and associated low emission efficiency, but all have inherent limitations [5-8]. A novel technique combining aspect ratio trapping and nano-ridge engineering [9-11] has allowed to demonstrate selective area growth of high-quality III-V material on silicon substrates without introducing thick buffer layers. This technique offers advantages in term of device scalability, integration density and fabrication cost compared to other integration methods. Thus far, most of this work focused on GaAs nano-ridge devices with InGaAs quantum wells (QWs) as the gain material. This limits the emission wavelength to 1100 nm. In optical interconnect applications, emission at 1.31 μm or 1.55 μm is more standard however. As we showed earlier, using InGaAs nano-ridge devices allow to grow QWs with larger Indium content, shifting the gain peak to longer wavelengths [11].To realize the large-volume integration, footprint reduction and device miniaturization are critical. In this paper, we used a photonic crystal (PC) cavity to reduce device dimensions. The cavity was designed to suppress out-of-plane light loss, leading to low lasing threshold and reduced power consumption.

2. LASER DESIGN

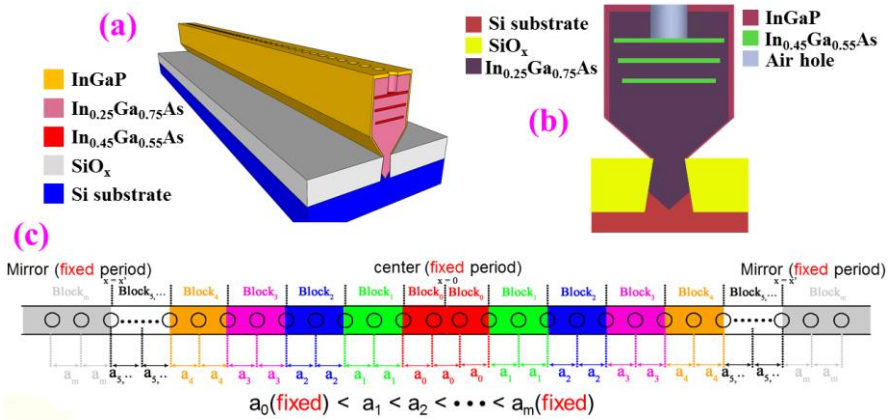

Figure 1(a). 3D photonic crystal nano-ridge cavity model. (b) Cross-section of the structure simulated with 3D-finite difference time domain (3D-FDTD) solver. (c) Top-view of the cavity model.

The PC nano-ridge cavity was designed using a 3D-finite difference time domain (3D-FDTD) solver. The simulation model and the cross-section of the simulated structure are shown in Figure 1(a) and 1(b). The air holes are reaching the top of the first QW layer, reaching a depth of approximately 180 nm. The design started with determining the fixed center period a_0 and mirror period a_m. Then, the periods (a_i, where i=1,2,3, …) between the fixed center a_0 and mirror a_m period were optimized to achieve a Gaussian envelope for the cavity mode field. As shown in Figure 1(c), the cavity was divided into blocks with the same period and the period increases from the center block to the mirror block, shifting down the bandgap.

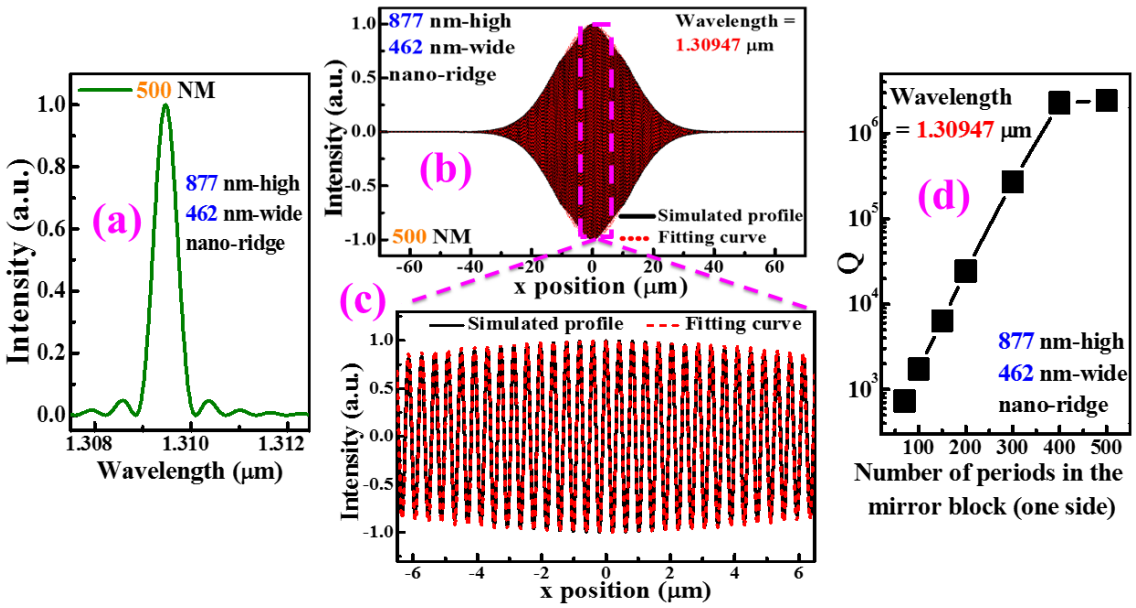

Figure 2(a) 3D-FDTD simulated spectrum from the 877 nm-high and 462 nm-wide photonic crystal nano-ridge cavity with 180 nm-deep etched holes and 500 periods in the mirror block at each side. (b) Electric field distribution along the light propagation direction at the wavelength of 1.30947 μm and the fit derived from the product of Gaussian and cosine function. (c) Detail from Figure 2(b). (d) Quality factor versus number of periods in the mirror block.

Figure 2(a) presents the simulated spectrum of 877 nm-high and 462 nm-wide nano-ridge with 500 periods in the mirror block at each side. The simulated resonance wavelength is located at 1.30947 μm. Figure 2(b) and (c) gives the simulated electric field distribution along the light propagation direction at this wavelength. The good overlap between the simulated electric field distribution and the fitted curve derived from the product of a Gaussian and cosine function

indicates the advanced design for manipulating out-plane light loss[12-14]. Figure 2(d) shows how the quality factor of the cavity increases with increasing number of periods (NM) in the mirror block, due to an enhanced light confinement. However, beyond 400 periods at each side, the Q-factor value stabilizes as the other light leakage mechanisms become dominant. To ensure sufficient reflection from the mirror block, 180 nm-deep air holes with 100, 130, 160, 190, 220, 250, 300, 350 and 400 periods in the mirror block at each side of the nano-ridge were incorporated into the final device design. Additionally, a second-order etched grating coupler with 200 periods was added at the front and back side of the cavity for later device characterization. Figure 3(a) and (b) give the simulated electric field profile in the PC nano-ridge cavity, showing the majority of the field is confined in a region of ±12 μm.

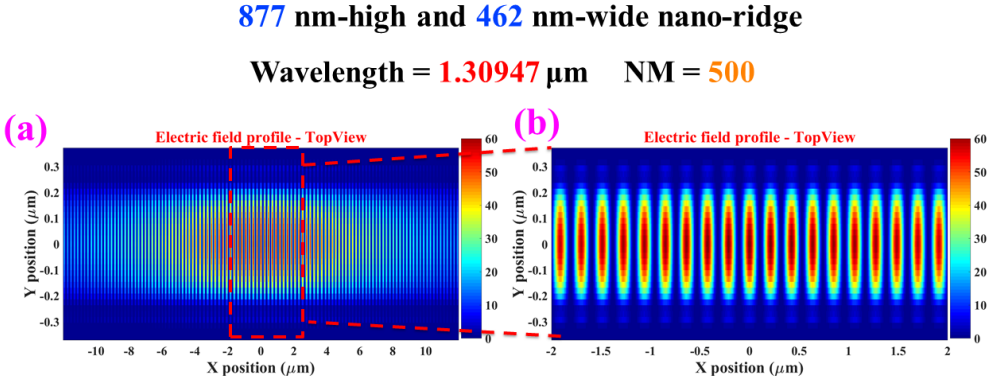

Figure 3(a) Simulated top-view electric field profile in the photonic crystal nano-ridge cavity. (b) Detail from Figure 3(a).

3. FABRICATON PROCESS

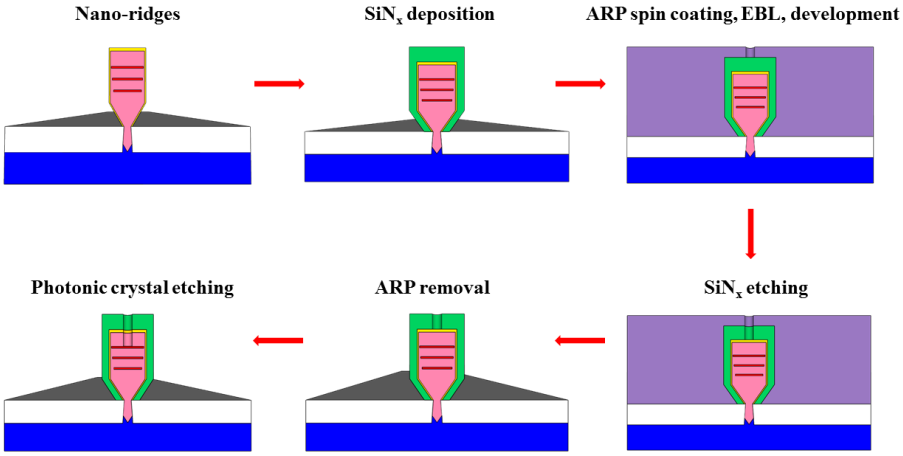

Figure 4 Process flow of photonic crystal nano-ridge cavity fabrication.

Following the design, the devices were fabricated starting from $In_{0.25}Ga_{0.75}As$ nano-ridges containing 3 $In_{0.45}Ga_{0.55}As$ QWs, passivated with an InGaP layer. The fabrication details are shown in Figure 4. The box-shaped nano-ridges were grown by metal organic vapor phase epitaxy (MOVPE) on a silicon substrate containing narrow trenches patterned in a SiO_2 layer. The details of the epitaxy process can be found in previous reports [9-11]. A ~100 nm SiN_x hard mask thin film was deposited on the nano-ridge using plasma-enhanced chemical vapor deposition (Advanced Vacuum Vision 310 PECVD, Plasma-Therm) before ARP resist spin coating for electron beam lithography (EBL, Voyager, Raith). Then, the PC cavities with different periods in the mirror block were patterned into the ARP resist. The patterned structures were transferred into the SiN_x hard mask thin film and nano-ridge by inductively coupled plasma reactive ion etching (ICP-RIE, Plasmalab System 100, Oxford) with CHF_3/O_2 and BCl_3/N_2, respectively. Figure 5(a) and (b) present top-view scanning electron microscope (SEM) images of the PC nano-ridge lasers, which demonstrates the process flow worked.

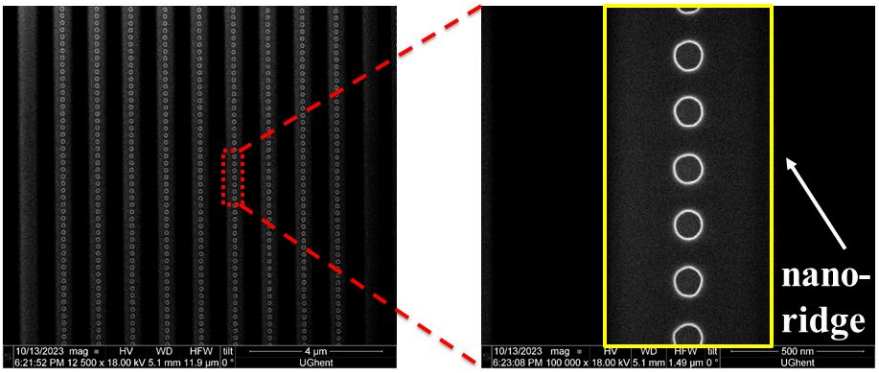

Figure 5(a) Top-view SEM image of photonic crystal nano-ridge laser. (b) Enlarged SEM image of the etched holes in one nano-ridge.

4. RESULTS AND DISCUSSION

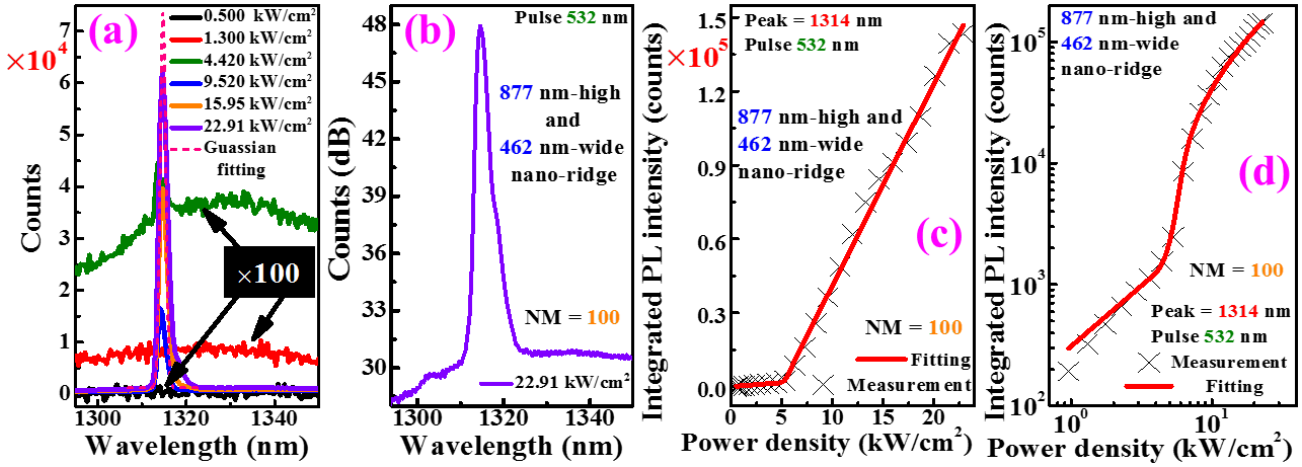

Figure 6(a) PL spectra from the photonic crystal nano-ridge laser with 100 periods in the mirror block at each side under different 532 nm pulsed pump power densities and a Gaussian fit applied to the spectrum under 22.91 kW/cm^2. (b) PL spectrum in dB scale from the same laser under 22.91 kW/cm^2. Light in (pump power density) - Light out (integrated PL intensity) curve on linear (c) and logarithmic (d) scale from the same laser, with fitted curve based on rate equations [15-16].

To characterize the optical properties, the device with 100 periods in the mirror block at each side and cavity length as small as 50 μm was excited by a Nd:YAG 532-nm nanosecond pulsed laser at room temperature. The emission from the device was collected and detected with a monochromator (KYMERA-328I-D2-SIL, Oxford instruments, Andor) and a water-cooled InGaAs detector (iDus, DU490A-1.7 Model, Oxford instruments, Andor). Figure 6(a) gives the photoluminescence (PL) spectra of this device under different 532 nm pulsed pumping. A lasing peak at 1314 nm appears at 4.42 kW/cm^2 and the peak intensity increases significantly as the pumping power density rises further. The linewidth of the laser, obtained from fitting a Gaussian function with the spectrum at 22.91 kW/cm^2, is 1.47 nm, and is believed to be limited by carrier dispersion during the pump pulse. Figure 6(b) shows a side-mode suppression ratio of more than 17 dB for this device at 22.91 kW/cm^2. Figure 6(c) and 6(d) show light in (pump power density) - light out (integrated PL intensity) curve on linear and logarithmic scale, together with a fitted curve obtained from the rate equations [15-16]. A clear change of slope and S-shaped curve are strong indicators of laser operation.

5. CONCLUSION

In conclusion, we fabricated compact photonic crystal $In_{0.45}Ga_{0.55}As/In_{0.25}Ga_{0.75}As$ nano-ridge lasers monolithically grown on a standard 300-mm Si wafer. The photonic crystal cavity consists of 180 nm-deep etched holes and the mirror block at each side comprises 100 periods. As a result of the enhanced light interaction in the photonic crystal, the lasing

was achieved in a device with a cavity length as small as 50 μm and with a remarkably low pulsed pumping power density threshold of 4.42 kW/cm^2. The laser exhibited a lasing peak with side-mode suppression ratio exceeding 17 dB and a linewidth as narrow as 1.47 nm at 22.91 kW/cm^2. This compact photonic crystal laser emitting at 1.31 μm opens up a promising path towards developing ultra-compact electrically-driven devices [17] for future high-density and massively scalable silicon photonic integrated circuits.

ACKNOWLEDGEMENT

This project has received funding from the European Union's Horizon 2020 research and innovation programme under grant agreement No. 884963 (ERC AdG NARIOS) and the China Scholarship Council, supported by imec's industry-affiliation Optical I/O R&D programme.

REFERENCES

[1] Zhiping Z., Bing Y. and Jurgen M., "On-chip light sources for silicon photonics," Light Sci. Appl. 4:e358 (2015).
[2] Daoxin D., Jared B. and John E B., "Passive technologies for future large-scale photonic integrated circuits on silicon: polarization handling, light non-reciprocity and loss reduction," Light Sci. Appl. 1:e1 (2012).
[3] David J. T., Frederic Y. G., Jean-Marc F. et al, "50-Gb/s Silicon Optical Modulator," IEEE Photon. Technol. Lett. 24(4), 234-236 (2012).
[4] Laurent V., Andreas P., Delphine M. et al, "Zero-bias 40Gbits germanium waveguide photodetector on silicon," Opt. Express 20(2), 1096-1101 (2012).
[5] Huiyun L., Jun Su L., Yan Z. et al, "Flip-chip integration of tilted VCSELs onto a silicon photonic integrated circuit," Opt. Express, 42, 5110-5112 (2017).
[6] Muhammad Rodlin B., Matthias B., Tobias H., et al, "Hybrid integration of silicon photonics circuits and InP lasers by photonic wire bonding," Optica 5 876-883 (2018).
[7] Jing Z., Grigorij M., Joan J., et al, "III-V-on-Si photonic integrated circuits realized using micro-transfer-printing," APL Photonics 4, 11803:1-10 (2019).
[8] Junjie Y., Pamela J., Fan C., et al, "Thin Ge buffer layer on silicon for integration of III-V on silicon," J. Cryst. Growth, 514, 109-113 (2019).
[9] Dries Van T., Yuting S., Marina B., et al, "Nano-ridge laser monolithically grown on (001) silicon," Future directions in silicon photonics, Chapter 8, 101, 283-304 (2019).
[10] Marina B., Yves M., Yoshiyuki I., et al, "Nano-Ridge Engineering of GaSb for the Integration of InAs/GaSb Heterostructures on 300 mm (001) Si," Crystals, 10, 330:1-19 (2020).
[11] Davide C., Marina B., Yuting S., et al., "Unique design approach to realize an O-band laser monolithically integrated on 300mm Si substrate by nano-ridge engineering," Opt. Express 30, 13510-13521 (2022).
[12] Y. Akahane, T. Asano, B. Song, et al., "High-Q photonic nanocavity in a two-dimensional photonic crystal", Nature. 425, 944-947 (2003).
[13] Y. Tanaka, T. Asano, and S. Noda, "Design of Photonic Crystal Nanocavity With Q-Factor of ~10^9", J. Lightw. Technol. 26, 11:1532-1539 (2008).
[14] E. Kuramochi, H. Taniyama and T. Tanabe et al., "Ultrahigh-Q one-dimensional photonic crystal nanocavities with modulated mode-gap barriers on SiO_2 claddings and on air claddings", Opt. Express 18, 15: 15859-15869 (2010).
[15] H. Yokoyama and S. D. Brorson, "Rate equation analysis of microcavity lasers," J. Appl. Phys. 66, 4801 (1989).
[16] K. A. Shore and M. Ogura, "Threshold characteristics of microcavity semiconductor lasers," Opt. Quantum Electron. 24, 209-213 (1992).
[17] Yannick De K., Charles C., Didit Y. et al, "GaAs nano-ridge laser diodes fully fabricated in a 300 mm CMOS pilot line," Nature, preprint version, 2023.